Unfalsified Switching Adaptive Voltage Control for Islanded Microgrids

Seyed Iman Habibi, Student Member, IEEE, Ali Bidram, Senior Member, IEEE

Abstract—Microgrid's voltage regulation is of particular importance during both grid-connected and islanded modes of operation. Especially, during the islanded mode, when the support from the upstream grid is lost, stable voltage regulation is vital for the reliable operation of critical loads. This paper proposes a robust and data-driven control approach for secondary voltage control of AC microgrids in the presence of uncertainties. To this end, unfalsified adaptive control (UAC) is utilized to select the best stabilizing controller from a set of pre-designed controllers with the minimum knowledge required from the microgrid. Two microgrid test systems are simulated in MATLAB to verify the effectiveness of the proposed method under different scenarios like load change and communication link failure.

Index Terms—Microgrid, secondary voltage control, switching control, unfalsified adaptive control.

NOMENCLATURE

v_{ref}	Reference voltage.	
v_{oi}	Terminal voltage magnitude of the i^{th} DG.	
ω_i	Operating angular frequency of the i^{th} DG.	
δ_i	Angle between i^{th} DG reference frame and the	
·	common reference frame.	
g_i	Pinning gain	
a_{ij}	Weight of the edge between node i and node	
	j in a communication graph.	
P_i	Active power of the i^{th} DG.	
Q_i	Reactive power of the i^{th} DG.	
i_{oi}	Terminal current magnitude of the i^{th} DG.	
i_{li}	Filter current of the i^{th} DG.	
V_{ni}	Voltage droop reference value of the i^{th} DG.	
ω_{ni}	Frequency droop reference value of the i^{th} DG.	
n_{Qi}	Voltage droop coefficient of the i^{th} DG.	
PI_{vci}	PI controller used for providing voltage and	
	reactive power ratio consensus.	
β_{ci}	Proportional coefficient of the PI_{vci} .	
α_{ci}	Integral coefficient of the PI_{vci} .	
PI_{vti}	PI controller used for tracking the reference	
	voltage.	
β_{ti} ,	Proportional coefficient of the PI_{vti} .	
α_{ti}	Integral coefficient of the PI_{vti} .	
v_{vci}	Auxiliary control input for PI_{vci} .	
v_{vti}	Auxiliary control input for PI_{vti} .	
C	Controller bank.	
$ar{V}_i$	Cost function for the i^{th} controller in the	
	controller bank of a single agent system.	

S.I. Habibi and A. Bidram are with the Department of Electrical and Computer Engineering, University of New Mexico, Albuquerque. USA. (Emails: habibi@unm.edu and bidram@unm.edu). This material is based upon work supported by the National Science Foundation EPSCoR Program under Award OIA-1757207.

\bar{V}_k	Multiagent cost function for the k^{th} DG.		
\tilde{r}_k	Fictitious reference signal of r for the k^{th}		
	controller in the controller bank.		
λ	Designing Parameter for the UAC.		

I. Introduction

A CCORDING to the Department of Energy, microgrids are a group of inter-connected loads and distributed generators (DGs) that are located in a specific electric boundary and can act as a fully controllable system component from the perspective of upstream electric grid [1]. Microgrids can facilitate the smooth integration of renewable energy resources such as wind turbine generators, photovoltaic systems, fuel cells, etc. and improve the reliability, efficiency, and resilience of power grids by incorporating information and communication technologies. Microgrids can operate autonomously from the upstream grid in an islanded mode. They can provide guaranteed stability and a continuous supply of power to the critical customers through their hierarchical control structure including primary, secondary, and tertiary control levels [2]–[4].

During the normal operation, microgrids are connected to an upstream grid where the upstream grid satisfies the voltage and frequency stability of the microgrid. However, entering the islanded mode, intentionally or unintentionally, can cause voltage and frequency instability in the microgrid. Primary control is deployed to maintain the voltage and frequency stability of the microgrid. However, after the islanding procedure, the microgrid's voltage and frequency slightly deviate from their nominal values. These deviations are compensated by the secondary control level to operate the microgrid at nominal voltage and frequency values [5]-[7]. According to [8], moreover, secondary control is responsible for reliable and economic operation of microgrid by finding the optimal or near optimal generation of DGs and accoridngly dispatching them. Conventionally, secondary control is implemented using a centralized communication structure. More recently, distributed secondary control approaches have been introduced to accommodate a more reliable and flexible voltage regulation and frequency restoration [9]-[12]. Due to the microgrid's distributed nature, the multi-agent control structure is a valuable approach for its control. In the distributed multiagent microgrid control system, all DGs communicate through a peer-to-peer communication network and each DG only needs its information and the information of DGs that can communicate to it directly [13]–[16].

In this paper, distributed secondary voltage control of microgrids is of concern. The stability of voltage control of microgrids depends on different factors including DG's primary control parameters, and microgrids' uncertainties, unknown dynamics, load changes, DGs' availability, etc. These factors can affect the performance of the microgrid voltage control system such that the voltage stability margin is violated which in turn results in the microgrid voltage instability. After a microgrid is islanded, adopting the distributed voltage control parameters that can guarantee the voltage stability is of paramount value. Conventional distributed secondary voltage control assumes fixed control parameters that are well suited for a specific condition of the system. However, with fixed control parameters, the microgrid may become unstable due to the uncertainties associated with the microgrid's dynamics, loads, and DGs. Therefore, robust and adaptive secondary voltage control of microgrids is of particular importance to improve their reliability and resilience.

The robust and adaptive secondary voltage control of microgrids has been investigated in [17]-[22]. In [17], a model free voltage secondary control using a multiple model adaptive approach is designed. The performance of this method heavily depends on the estimation of unmodeled dynamics. In [18], a robust distributed secondary controller is designed for voltage/frequency restoration and reactive/active powersharing of an islanded microgrid in the presence of communication uncertainties. Reference [19] aims to attenuate the parametric uncertainties of a DC microgrid using the linear matrix inequality (LMI) approach. Reference [20] designed a robust finite-time controller to improve the robustness and stability of secondary control of a microgrid against various uncertainties. Reference [21] proposes an analytical method to handle communication delays for the secondary voltage control of microgrids. In [22], a model predictive control based optimization is used to propose a supervisory secondary voltage and frequency method.

In this paper, unfalsified adaptive control (UAC) is utilized to accommodate a robust and adaptive control for distributed secondary voltage control of microgrids. Reference [23] proposes the concept of UAC in the literature for the first time. The stability proof of this method is presented in [24], [25]. In [26], the multi-model UAC is proposed which requires a model bank in addition to the controller bank. In [27], a fuzzy cost function is introduced for UAC to improve its performance. UAC is a model-free, data-driven, robust, and adaptive methodology which uses input-output plant data to control and evaluate the performance and stability of an uncertain plant. UAC assumes a group of controllers in the controller bank that are predesigned for different conditions of the system and aims to select the most optimized controller according to the control objectives. At each time instance, UAC only puts one controller in the loop. Other controllers are called outside loop controllers in the controller bank. Different algorithms have been proposed in the literature to implement UAC. These algorithms are ϵ - hysteresis, Increasing Cost Level Algorithm (ICLA), and Linear Increasing Cost Level Algorithm (LICLA) [28]. In this paper, LICLA is used since it does not require a monotone cost function and has a better performance compared to its peers. Adopting a proper cost function to accommodate a stable operation in the system is

of particular significance. To ensure stability, The cost function needs to be cost-detectable [24]. Cost-detectability denotes the ability of cost function in identifying the instability in the system by using only input-output plant data. The cost function is based on the fictitious reference signal, which is important from real-time and data-driven points of view. This signal is the answer to the following question: "If the outside loop controller had been in the loop, what reference input would have generated the input-output plant data?"

The literature review highlights some of the gaps in the existing microgrid secondary voltage control techniques that are addressed in this paper. The existing secondary control techniques only rely on a single control protocol which may make the system unstable under some conditions (e.g., change of microgrid load). Moreover, there is a need for a robust and adaptive voltage regulation with the least possible assumptions and information from the microgrid. To address these gaps, the contributions of this paper are summarized as follows:

- It is the first time that UAC is introduced to the microgrid secondary voltage control for guaranteeing the voltage stability of microgrid under a wide range of operating conditions.
- The UAC-based secondary voltage control accommodates a robust and adaptive control framework that requires minimal information from the microgrid system. The UAC engine is responsible for selecting the appropriate distributed control parameters to ensure the stability of control system. The proposed control system accounts for the uncertainties in the microgrid system.
- A cost-detectable cost function for UAC in a multiagent system structure is proposed which helps the UAC algorithm find the most appropriate controller for the microgrid secondary voltage control.

The structure of this paper is as follows: Section II discusses some preliminaries on microgrid dynamics and secondary voltage control. Section III explains the required preliminaries of UAC. In Section IV, the UAC is proposed for secondary voltage control of microgrids. In Section V, simulation results are presented to verify the effectiveness of the proposed voltage secondary control algorithm. Section VI concludes the paper.

II. MICROGRID'S PRELIMINARIES

A. Microgrid Dynamic Model

The microgrid system considered in this paper consists of DGs, loads, and the lines interconnecting them, as well as a communication network and nested control loops. All the DGs in this paper are assumed to be inverter-based ones (see Fig. 1). As seen in Fig. 1, an inverter-based DG includes an inverter bridge, a primary DC power source, power controller, current controller, and voltage controller. All DGs utilize a communication network to exchange data among them. It is assumed that the communication network contains at least one directed spanning tree.

In this paper, the microgrid's dynamic used for simulation is completely nonlinear, which makes it very close to a real microgrid in practice. In this paper, the nonlinear dynamical

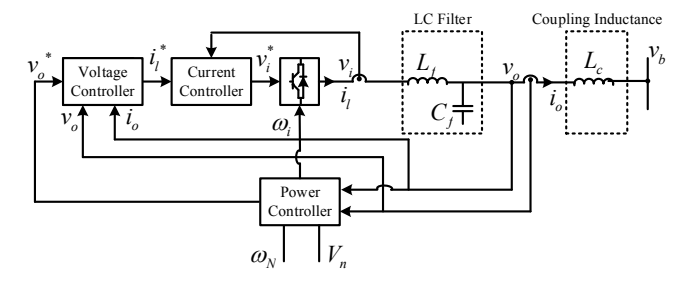


Fig. 1. An inverter-based DG.

model of an inverter-based microgrid discussed in [11] is utilized. The nonlinear dynamical model of an inverter-based DG can be formulated in d-q reference frame as

$$\begin{cases} \frac{dx_i}{dt} = f_i(x_i) + k_i(x_i)D_i + g_i(x_i)u_i \\ y_i = h_i(x_i) \end{cases}$$
 (1)

where

$$x_{i} = \begin{bmatrix} \delta_{i} & P_{i} & Q_{i} & \phi_{di} & \phi_{qi} & \gamma_{di} & \gamma_{qi} & i_{ldi} \\ i_{lqi} & v_{odi} & v_{oqi} & i_{odi} & i_{oqi} \end{bmatrix}^{T}$$

$$u_{i} = \begin{bmatrix} V_{ni} & \omega_{ni} \end{bmatrix}^{T}$$

$$y_{i} = \begin{bmatrix} \omega_{i} & v_{oi} \end{bmatrix}^{T}$$

where δ_i is the angle between i^{th} DG reference frame and the common reference frame, P_i is the active power, and Q_i is the reactive power. State variables ϕ_{dqi} and γ_{dqi} are the direct and quadrature components of state variables related to inner voltage and current controllers, respectively. State variables v_{odqi} , i_{ldqi} , and i_{odqi} are the direct and quadrature components of output voltage, filter current, and output current of DG_i , respectively. Matrices f_i , k_i , g_i , and h_i and vector D_i are all defined in [11]. Variables v_{oi} and ω_i are the DG's terminal voltage magnitude and operating frequency; variables V_{ni} and ω_{ni} are the voltage and frequency droop reference values that will be described in Section IV.

Since the focus of this paper is on the secondary control of an islanded microgrid, all inverters are assumed to be operating in the grid-forming mode. In this mode, the inverters can operate at their own operating voltage and frequency in order to effectively maintain microgrid's stability right after the islanding occurs. According to [29]–[34], in the grid-forming mode, inverters do not require a phase locked loop (PLL) to operate. However, a PLL is an essential part of a grid-following inverter in order to effectively synchronize the inverter to the rest of microgrid.

B. Distributed Secondary Voltage Control

The microgrid voltage control system in this paper consists of primary and secondary controls. Primary control guarantees that the voltage of the microgrid is stable after entering islanding mode. The secondary control which is the focus of this paper aims to accommodate proper voltage/frequency tracking and active/reactive power sharing in a microgrid. At each inverter-based DG, the primary control includes the

voltage and frequency droop characteristics. The voltage droop characteristic is

$$v_{oi}^* = V_{ni} - n_{Qi}Q_i \tag{2}$$

where v_{oi}^* is the reference for the internal voltage and current control loops of DG to control the DG's terminal voltage magnitude v_{oi} ; The term V_{ni} is the voltage droop reference value; The coefficient n_{Qi} is the voltage droop coefficient, and Q_i is the reactive power of i^{th} DG. The voltage droop coefficients are chosen based on the reactive power ratings of DGs.

The voltage droop control is only able to maintain the voltage stability of the microgrid. Using voltage droop control, the microgrid's voltage stays within a stable range but with a slight deviation from the nominal voltage, v_{nom} . The objectives of the secondary voltage control are (i) to restore DGs' voltage magnitudes to a reference voltage, v_{ref} (v_{ref} can be selected as v_{nom} or can be tuned to control the microgrid's critical bus voltage, v_c), and (ii) to synchronize all the DG's reactive power ratios to the same values enforced by the primary voltage droop control. To have secondary control regulate the voltage of a critical bus of microgrid, v_{ref} is selected as [6]

$$v_{re} = \alpha_{Cr} \int (v_{nom} - v_c) dt + \beta_{Cr} (v_{nom} - v_c)$$
 (3)

where β_{C_r} and α_{Cr} are the proportional and integral coefficients of the PI controller for v_{ref} , respectively. This PI controller is referred to as PI_{Cr} .

The secondary voltage control problem can be interpreted as a multi-agent system. Differentiating the voltage droop characteristic of i^{th} DG, one has

$$\frac{dV_{ni}}{dt} = \frac{dv_{oi}^*}{dt} + n_{Q_i} \frac{dQ_i}{dt} \tag{4}$$

In this paper, the voltage droop reference value V_{ni} is defined as

$$V_{ni} = \alpha_{ci} \int v_{vci} dt + \beta_{ci} v_{vci} + \alpha_{ti} \int v_{vti} dt + \beta_{ti} v_{vti}$$
 (5)

where β_{ci} and α_{ci} are the proportional and integral coefficients of the PI controller used for providing voltage, v_{oi} , and reactive power ratio, $n_{Q_i}Q_i$, consensus, respectively. This PI controller is referred to as PI_{vc} . β_{ti} and α_{ti} are the proportional and integral coefficients of the PI controller used for tracking the reference voltage v_{ref} , respectively. This PI controller is referred to as PI_{vt} . The auxiliary control inputs v_{vci} and v_{vti} are defined as [6]

$$v_{vci} = \sum_{j \in N_i} a_{ij} (v_{oj} - v_{oi}) + \sum_{j \in N_i} (n_{Q_j} Q_j - n_{Qi} Q_i)$$
(6)

$$v_{vti} = g_i(v_{ref} - v_{oi}) \tag{7}$$

where g_i is the pinning gain and is only nonzero for the DGs that have access to v_{ref} . a_{ij} is the weight of the communication graph edge between i^{th} and j^{th} DGs. The auxiliary control input v_{vci} is available on all DGs and is responsible for providing voltage and reactive power ratio consensus among DGs. The auxiliary control input v_{vti} is only active on the DGs that have access to v_{ref} , and is responsible

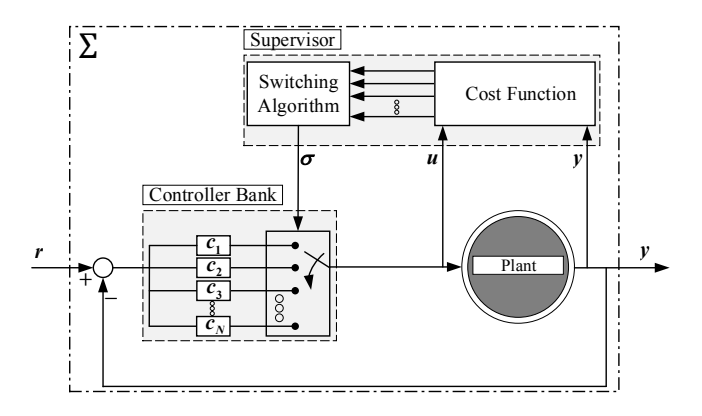


Fig. 2. Block diagram of switching adaptive control.

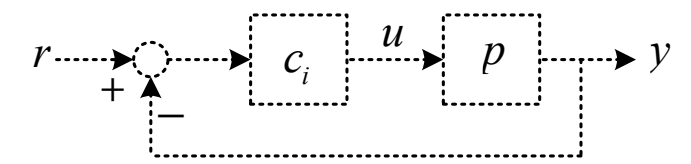


Fig. 3. Imaginary feedback loop.

for regulating the microgrid voltage. To avoid the issue of single point of failure, more than one DG can have access to v_{ref} . This means that if one of those DGs loses its access to v_{ref} , the remaining ones can safely use v_{ref} to synchronize the voltage of critical bus to the nominal voltage of microgrid.

III. UNFALSIFIED ADAPTIVE CONTROL

The overall block diagram of a switching adaptive control system is illustrated in Fig. 2. As seen, a switching adaptive control system contains a controller bank, an unknown plant p, and a supervisor. The controller bank is defined as follows,

$$C = \left\{ c_i(s) = \frac{S_i(s)}{R_i(s)}, i = 1, ..., N \right\}$$
 (8)

where R_i and S_i are polynomials and N denotes the number of existing controllers in the controller bank. The active controller selected by the switching algorithm at time t is denoted by $c_{\sigma(t)}$.

UAC is a switching adaptive control that requires the minimum knowledge from the plant model. At each time instance, there is only one active controller in the loop and other controllers in the controller bank are called outside-loop controllers. In UAC, the supervisor's role is to select a stabilizing and appropriate controller according to the control objectives. The important feature of UAC is that the supervisor only requires input-output plant data (u,y) and is not dependent on the plant model. This unit involves a switching algorithm and a cost function. Conventionally, the cost function is selected as

$$V_i(t) = \frac{\|\tilde{r}_i - y\|_{[0,t]} + \|u\|_{[0,t]}}{\alpha + \|\tilde{r}_i\|_{[0,t]}}$$
(9)

where V_i and \tilde{r}_i are the cost function and the fictitious reference signal of i^{th} controller in the controller bank, respectively. In this paper, tilde symbol is used to define the

fictitious value of a variable. u and y are the input-output plant data. α is a positive real value. This paper introduces new cost functions for the proposed UAC-based distributed secondary voltage control of microgids which are described in Section IV.

Definition: Fictitious reference signal of i^{th} controller, \tilde{r}_i , is an imaginary signal that regenerates the input-output data of an unknown plant p (See Fig. 3).

Assuming that the controllers in the controller bank are non-minimum phase, this signal can be calculated as follows,

$$\tilde{r}_i(t) = c_i^{-1}(s)u(t) + y(t) \tag{10}$$

It should be noted that the controllers used for distributed secondary voltage control are usually non-minimum phase. However, if there is at least one minimum phase controller in the controller bank, the method proposed in [25] can be utilized to calculate the fictitious reference signal.

The switching algorithm evaluates the performance of the active and the outside-loop controllers according to their cost function. The algorithm used in this paper is LICLA which can be seen in the following Algorithm [28],

Algorithm: LICLA

- Initialization:
- $\lambda \leftarrow \lambda_0 \ge 0, \Delta \lambda > 0, C = \{c_1, c_2, ..., c_N\}, c_{\sigma}(t) \in C, t \leftarrow 0$
- 2 $t \leftarrow t + 1$, collect data, calculate V.
- **3** If $V_{\sigma(t)} > \lambda(t)$ Then $C \leftarrow C \setminus c_{\sigma(t-1)} \Rightarrow c_{\sigma(t-1)}$ is falsified.
- 4 If $C \in \emptyset$ Then $C \leftarrow \{c_1, c_2, ..., c_N\}$ endif
- 5 $c_{\sigma(t)} = \arg\min_{\forall c, \in C} V_i(t), \lambda \leftarrow \lambda + \Delta \lambda$
- 6 else
- 7 $c_{\sigma(t)} = c_{\sigma(t-1)}$
- 8 endif
- 9 Back to line 2.

The active controller is falsified by input-output plant data if its cost function is greater than a positive value $\lambda(t)$. The falsified controller is removed from the controller bank and the controller with the lowest value cost function is replaced with the falsified controller. If the controller bank becomes empty, all the controllers are pushed back to the controller bank.

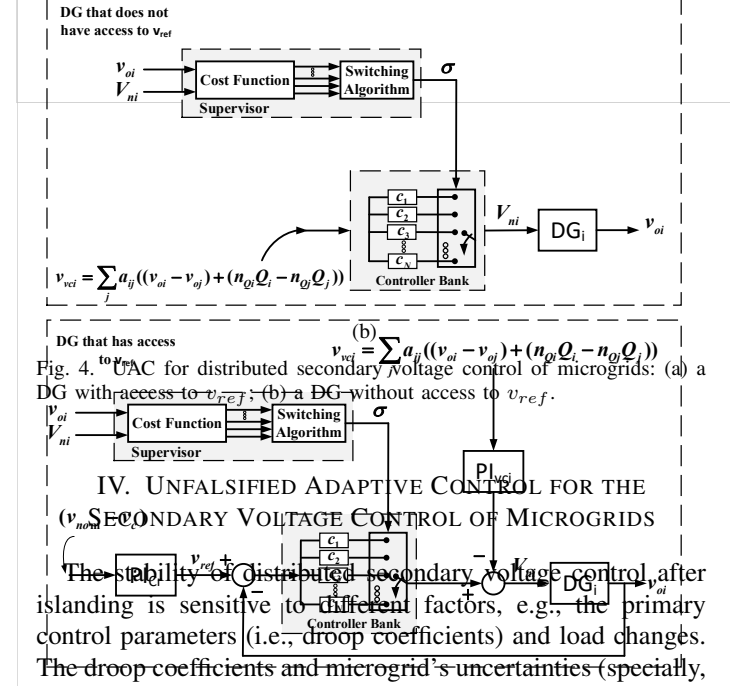
Definition: If at least one stabilizing controller exists in the controller bank, the adaptive control problem is feasible.

Definition: Given the input-output plant data (u, y) and a closed-loop system with reference input r, the closed-loop system is stable if, for all $r \in l_{2e}$, m, n > 0 exist such that,

$$||u||_{[0,t]} + ||y||_{[0,t]} < m||r||_{[0,t]} + n$$
 (11)

UAC considers assumptions on the cost function instead of assumptions on the plant. For UAC, to be stabilizing, the cost function needs to be cost-detectable. The following statement must be true for a cost detectable cost function: The function $V_f(.)$ is bounded if and only if (p/c_f) is stable, where c_f is the final controller in the loop and $V_f(.)$ is the cost function of the final controller in the loop. System (p/c_f) is a closed-loop system with p and c_f in its forward path [26].

(a)



from loads) can affect the performance of the voltage control

such that the voltage stability margin is violated. Therefore,

after the microgrid islanding, adopting the distributed voltage

control parameters that can guarantee the voltage stability is

of paramount value. In this section, the UAC is proposed for

the distributed secondary voltage control of AC microgrids.

To this end, the conventional UAC, proposed in Section IV, is

reformulated for a multi-agent system and a new cost function

is defined accordingly. In the proposed UAC-based distributed

secondary voltage control, UAC can be located on any of the

DGs. Depending on the access of DG to v_{ref} , two different

cost functions are proposed which are elaborated as follows: If a DG has access to v_{ref} , then UAC selects the proper PI_{vt} in (5). To avoid the issue of single point of failure, more than one DG can have access to v_{ref} . In Fig. 4a, the block diagram of UAC integrated into a DG with access to v_{ref} is illustrated. In this figure, N is the number of existing controllers in the UAC controller bank. Also, $\{c_1, c_2, ..., c_N\}$ denotes the set of controllers in the controller bank and σ is the index of the selected controller. The UAC ensures the stability of this loop if the problem is feasible, i.e., there is at least one stabilizing controller in the controller bank. If the microgrid dynamics change and the active controller becomes

destabilizing, the UAC identifies this issue and changes the active controller to a stabilizing one. In this paper, the cost function of UAC is reformulated for the microgrid's distributed secondary voltage control system. The UAC cost function for a DG with access to v_{ref} is formulated as

$$\bar{V}_k(t) = \frac{\|\tilde{r}_k - y\|_{[0,t]} + \|u\|_{[0,t]}}{\alpha + \|\tilde{r}_k\|_{[0,t]} + \tilde{v}_{vc,k}}$$
(12)

where \tilde{r}_k denotes the fictitious signal of r for the k^{th} controller in the controller bank. Herein, the bar symbol is used to describe the cost function in a multiagent system. r for the DG that has access to the v_{ref} is equivalent to v_{ref} . α is a positive real value. The term $\tilde{v}_{vc,k}$ is equal to $\sum_{j\in N_i} \|\tilde{v}_{vcj,k}\|_{[0,t]}^2$. The term $\tilde{v}_{vcj,k}$ is the fictitious signal of v_{vcj} , defined in (6), for k^{th} controller in the controller bank.

Theorem: Consider a DG that has access to v_{ref} (or equivalently r), input-output plant data (V_{ni}, v_{oi}) , the cost function $\bar{V}(t) = \{\bar{V}_k(t)|k=1,...,N\}$ defined in (12), and the auxiliary control inputs v_{vej} as disturbance signals. If the problem is feasible and the pair of cost function and the controller bank is cost detectable, then the UAC system is stable.

Proof: The proof is provided in the Appendix.

If a DG doesn't have access to v_{ref} , then UAC selects the proper PI_{vc} in (5). In Fig. 4b, the block diagram of UAC integrated into a DG without access to v_{ref} is illustrated. The cost function in this case is defined as

$$\bar{V}_k(t) = \frac{\|\tilde{v}_{vci,k}\|_{[0,t]} + \|u\|_{[0,t]}}{\alpha + \tilde{v}_{vc,k}}$$
(13)

where $\tilde{v}_{vci,k}$ is the fictitious signal of v_{vci} and $\tilde{v}_{vc,k} = \sum_{j \in N_i} \|\tilde{v}_{vcj,k}\|_{[0,t]}$. α is a positive real value

Remark: The proposed unfalsified adaptive control approach has separate solutions for the DGs with v_{ref} access and DGs without v_{ref} access. For the DGs with v_{ref} access, the cost function in (12) is used, while the DGs without v_{ref} access utilize the cost function in (13). As discussed earlier, to increase the reliability of distributed control of microgrid, more than one DG can have access to v_{ref} . Assuming that two DGs have access to v_{ref} , both DGs can have their own UAC control in place using the cost function in (12). Doing so, if one of the DGs with v_{ref} access is outaged or loses its access to v_{ref} , the UAC of the other DG with v_{ref} access can take action and ensure voltage regulation and microgrid stability. Moreover, DGs without v_{ref} access can also have their own UAC using the cost function in (13) to effectively select an stabilizing controller based on the microgrid condition if all of the DGs with v_{ref} access are compromised.

V. SIMULATION RESULTS

In this section, the effectiveness of the proposed UAC-based distributed secondary voltage control is verified by simulating two different microgrid systems under different conditions like load change and droop coefficient change. Moreover, the impact of communication link failure and delay is studied. The first microgrid test system is a 4 DG microgrid while the second one is a 20 DG microgrid test system.

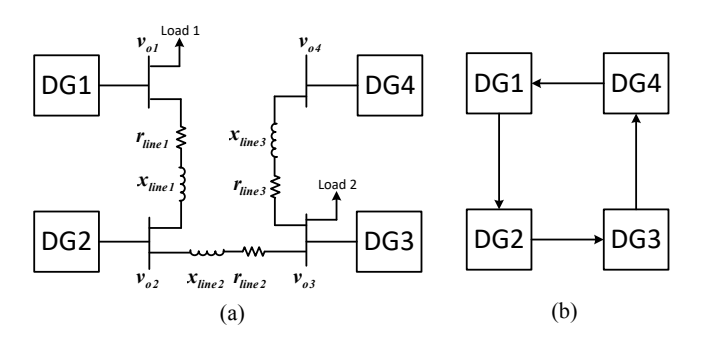
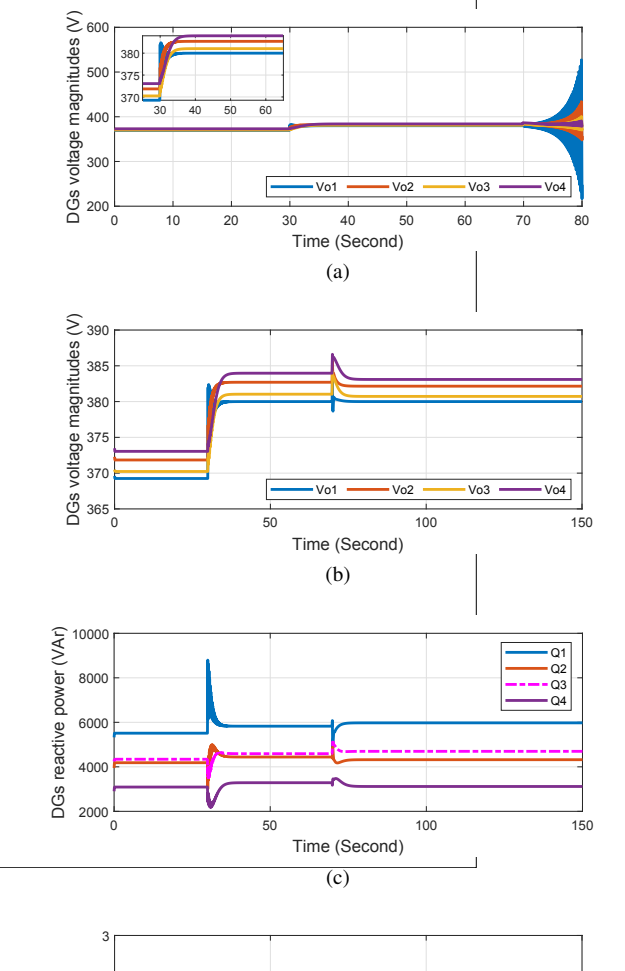


Fig. 5. Case Study A: (a) microgrid diagram; (b) communication graph.

TABLE I THE PARAMETERS OF 4 DG MICROGRID.

380 V, 50 Hz
9.4e - 5
[1.95, 1.95, 2.25, 2.25]e - 3
[1.3, 1.3, 1.5, 1.5]e - 3
[1, 1, 1, 1]e - 3
144.4 kW
144.4 kVAr
0.5Ω
8Ω
0.5Ω
8Ω
$5e-2\Omega$
$1.6e - 3 \Omega$
[0.05, 10.5, 390, 16e3]
[.35 mH, 50 μ F, 0.35 mH]



50

A. Case Study A

The microgrid test system for Case Study A is shown in Fig. 5a. The communication graph for the secondary distributed control is illustrated in Fig. 5b.

1) Case Study A1 - UAC with Voltage Droop Coefficient Change when UAC is Located on DG1: In this section, the change in the voltage droop coefficients of Case Study A is analysed. The distributed secondary control of microgrids utilizes a communication network which makes the secondary control system accessible by cyber attackers. The attacker can access to the primary controller of the DGs and change their droop coefficients. The parameters of the microgrid are provided in Table I. The loads are constant and use $[R_{load12}, R_{load22}, X_{load12}, X_{load22}]$ values in Table I. The UAC is located on DG1 that has access to v_{ref} . It is assumed that the microgrid goes to islanding mode at t = 29.9 s. The controller bank of the UAC includes the following controllers, $c_1 = (2 - z^{-1})/(1 - z^{-1}), c_2 = (0.5 + 0.4z^{-1})/(1 - z^{-1}),$ where z^{-1} is the unit backward operator. Controllers c_1 and c_2 are stabilizing controllers designed for voltage droop coefficients $[n_{Q11}, n_{Q21}, n_{Q31}, n_{Q41}]$ and $[n_{Q12}, n_{Q22}, n_{Q32}, n_{Q42}]$, respectively. These droop coefficients are provided in Table I. Between t = 29.9 s and t = 69.9 s, it is assumed that the voltage droop coefficients of DGs are $[n_{Q11}, n_{Q21}, n_{Q31}, n_{Q41}]$. At t = 69.9 s, the voltage droop coefficients of DGs are changed to $[n_{Q12}, n_{Q22}, n_{Q32}, n_{Q42}]$. The initial active controller is c_1 . For each microgrid condition, the stabilizing controller is designed as follows: First, the integral coefficient

Switching 100 Time (Second)

Fig. 6. Results for Case Study A1: (a) DGs' voltage magnitudes using conventional control; (b) DGs' voltage magnitudes using UAC on DG1 with $\lambda_0 = 0.1$; (c) DGs' reactive powers using UAC on DG1 with $\lambda_0 = 0.1$; (d) controller switching instance using UAC on DG1 with $\lambda_0 = 0.1$.

of PI controller is set to zero and the proportional coefficient is increased until the output oscillates with a constant period T_u . This ultimate coefficient is called K_u . Then, a proportional coefficient that is smaller than K_u is selected so that the desired stability margin is acquired. Finally, an integral coefficient that is smaller than T_u is selected so that the desired response is achieved.

First, the conventional secondary control is used. The controller c_1 is used for the whole simulation. Between t = 29.9 s and t = 69.9 s, the controller c_1 accommodates a stable voltage regulation. After t = 69.9 s when the droop coefficients are changed to $[n_{Q12}, n_{Q22}, n_{Q32}, n_{Q42}]$, the controller c_1 results in the microgrid voltage instability (See Fig. 6a).

Then, it is assumed that DG1 is equipped with UAC. The designing parameter λ_0 in LICLA algorithm is set to

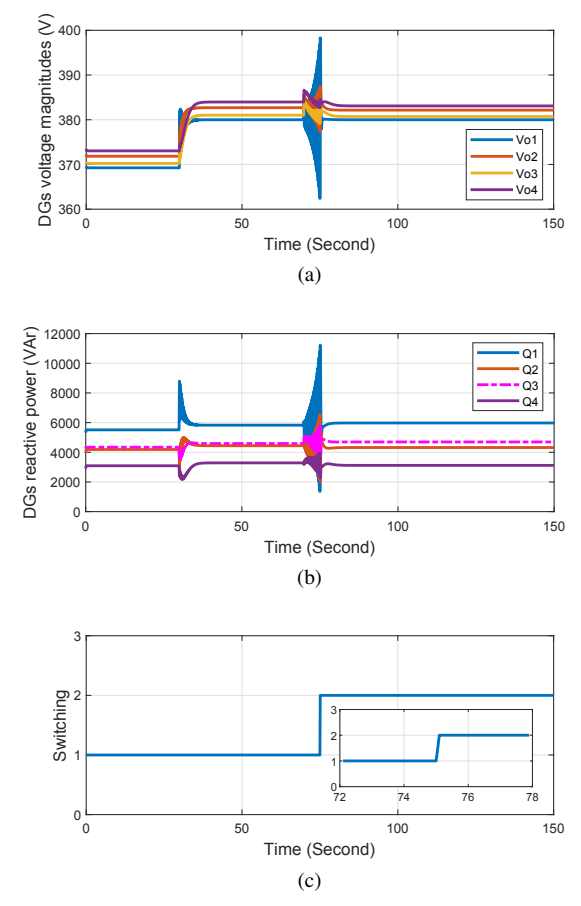


Fig. 7. UAC Results for Case Study A1 with $\lambda_0 = 0.9$: (a) DGs' voltage magnitudes; (b) DGs' reactive powers; (c) controller switching instance.

0.1. The UAC notices that at $t=69.9~\rm s$ the controller c_1 results in the microgrid's instability and at $t=70~\rm s$ switches to the stabilizing controller c_2 fast enough before the microgrid stability margins are violated. The DGs' voltage magnitudes, reactive powers, and controller switching instance are illustrated in Figs. 6b, 6c, and 6d, respectively. Figs. 6b and 6c show that UAC can effectively select the stabilizing controller and the DG's voltage and reactive powers are within stable ranges. Moreover, microgrid's voltages are synchronized to the microgrid nominal voltage. As seen in Fig. 6d, after $t=69.9~\rm s$, initially an unstable controller c_1 is the active controller. However, UAC detects the unstable controller and replaces it with the stabilizer controller in $0.1~\rm s$ at $t=70~\rm s$.

The above scenario is also simulated when the parameter λ_0 in LICLA algorithm is set to 0.9. Parameter λ_0 can impact on the response of UAC for identifying the stabilizing controller. As seen in Fig. 7, the UAC notices the instability slower than before when $\lambda_0=0.9$. The UAC replaces the active controller with the stabilizer one in 5.2 s at t=75.1 s.

2) Case Study A2 - UAC with Voltage Droop Coefficient Change when UAC is Located on DG3 and a DG with Access to v_{ref} Loses Its Access: The UAC can be used for a DG that does not have access to v_{ref} . Herein, UAC is installed on DG3. The controller bank of the UAC includes the following controllers, $c_1 = (1.1 - 1z^{-1})/(1 - z^{-1})$, $c_2 = (0.15 - 0.1z^{-1})/(1 - z^{-1})$. Controllers c_1 and c_2

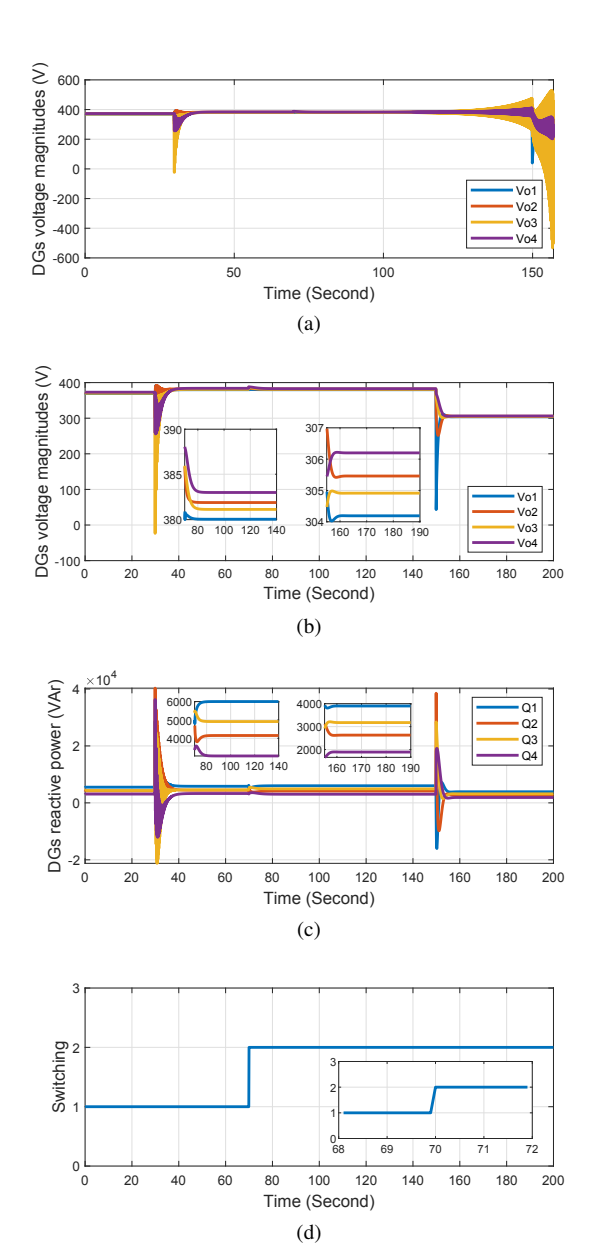


Fig. 8. Results for Case Study A2 when UAC is on DG3: (a) DGs' voltage magnitudes using conventional control; (b) DGs' voltage magnitudes using UAC; (b) DGs reactive powers using UAC; (c) controller switching instance.

are stabilizing controllers designed for voltage droop coefficients $[n_{Q11}, n_{Q21}, n_{Q31}, n_{Q41}]$ and $[n_{Q13}, n_{Q23}, n_{Q33}, n_{Q43}]$, respectively. UAC uses the cost function formulated in (13). The microgrid goes into islanding mode at $t=29.9~\rm s$. The voltage droop coefficient change is according to Table I and it occurs at $t=69.9~\rm s$. After $t=149.9~\rm s$, the DG that has access to v_{ref} loses its access. Therefore, after $t=149.9~\rm s$, no DG has access to v_{ref} . The simulation results are shown in Fig. 8. As seen, the UAC on DG3 successfully selects the stabilizer controller after voltage droop coefficients change. Moreover, with the selected controller, microgrid can still maintain its stability after DG1 loses its access to v_{ref} .

3) Case Study A3 - UAC with Voltage Droop Coefficient Change and Communication Failure and Delay: To show the effectiveness of the proposed method under communication link delay, a delay of 0.1 s is applied to all of the

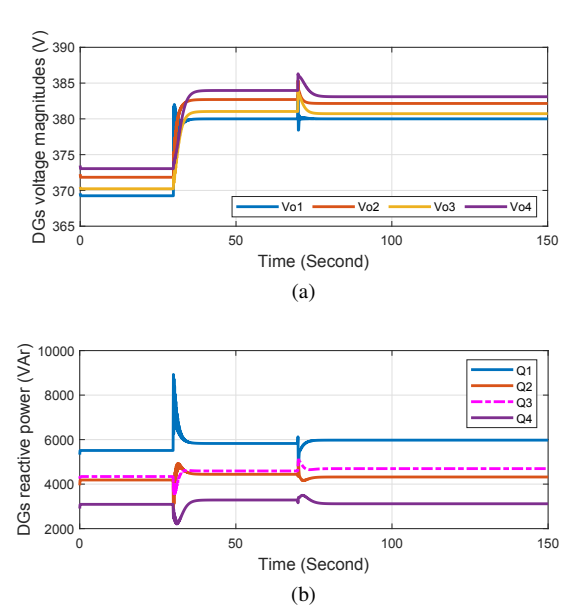
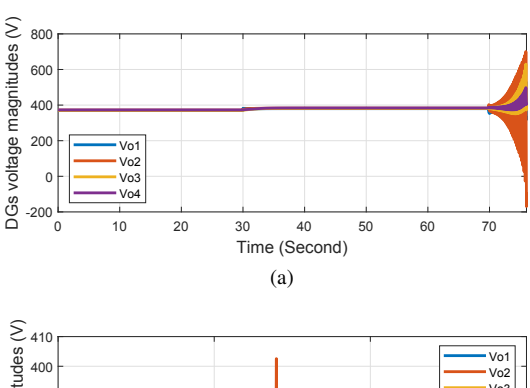


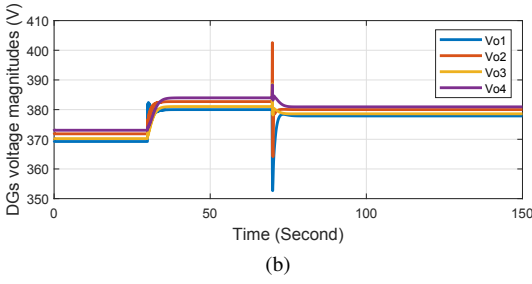
Fig. 9. UAC Results for Case Study A3 with communication link delay and failure: (a) DGs' voltage magnitudes; (b) DGs' reactive powers.

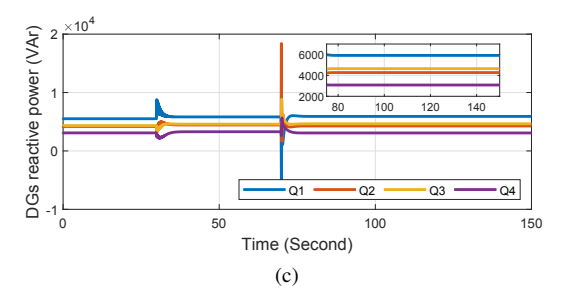
communication links. Herein, a scenario similar to the droop coefficient change scenario in Section V.A.1 is considered. The droop coefficient change occurs at t = 69.9 s. UAC is also located on DG1. The islanding occurs at t=29.9 s.Moreover, a communication link failure pattern is considered for the communication network that starts at t = 49.9 s. In this pattern, it is assumed that, first for a period of 0.1 s, the communication links have no failures. Then, for a period of 0.1 s, the communication link between DG1 and DG4 fails. Finally, for a period of 0.1 s, two communication links between DG1 and DG4 and between DG3 and DG4 fail. This communication failure pattern repeats until the end of the simulation. As seen in Fig. 9, the UAC can successfully select the stabilizer controller even in the presence of voltage droop coefficients change, communication delay, and communication failure.

4) Case Study A4 - UAC with Voltage Droop Coefficient Change when a DG with Access to v_{ref} Loses Its Access: In this section, it is assumed that two DGs have access to v_{ref} . The UAC has two controller in the controller bank. The controller bank includes, $c_1 = (2.5 - z^{-1})/(1 - z^{-1}), c_2 =$ $(0.5 + 0.4z^{-1})/(1 - z^{-1})$. Controller c_1 and c_2 are the stabilizing controllers designed for voltage droop coefficients $[n_{Q11}, n_{Q21}, n_{Q31}, n_{Q41}]$ and $[n_{Q12}, n_{Q22}, n_{Q32}, n_{Q42}]$, respectively. The initial active controller is c_1 . The microgrid goes to islanding mode at t = 29.9 s. Between t = 29.9 s and t = 69.9 s both DG1 and DG2 have access to v_{ref} . At t = 69.9 s, the droop coefficient change occurs. Also, at this time DG1 loses its access to v_{ref} . Therefore, after $t=69.9~\mathrm{s}$ only DG2 has access to v_{ref} . As seen in Fig. 10, the UAC on DG2 successfully selects the stabilizer controller after droop coefficient change and DG1 loses its access to v_{ref} .

The above scenario is also simulated when both DG1 and DG2 lose their access to v_{ref} at t=29.9 s. It should be also noted that even if all DGs lose their access to v_{ref} , the microgrid can still maintain its stability. However, in this case,







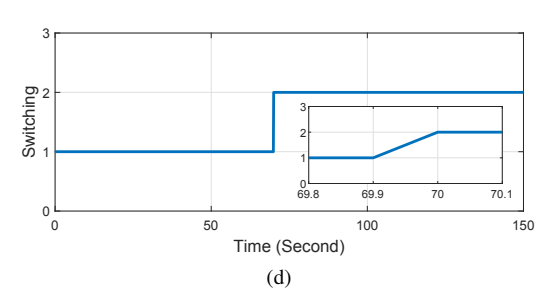


Fig. 10. UAC Results for Case Study A4 with failure in one of the DGs that has acces to v_{ref} : (a) DGs' voltage magnitudes using conventional method; (b) DGs' voltage magnitudes using UAC; (c) DGs' reactive powers; (d) controller switching instance.

the microgrid voltage is not regulated. This is shown in Fig. 11.

5) Case Study A5 - UAC with Load Change: Consider the 4 DG microgrid with constant droop coefficients $[n_{Q12}, n_{Q22}, n_{Q32}, n_{Q42}]$ but variable loads. It is assumed that the microgrid goes to islanding mode at t=29.9 s. Between t=0 s and t=69.9 s, it is assumed that loads of the microgrid are RX_1 . At t=69.9 s, the loads are changed to RX_2 , where

$$\begin{split} RX_1 &= [R_{load11}, R_{load21}, X_{load11}, X_{load21}], \\ RX_2 &= [R_{load12}, R_{load22}, X_{load12}, X_{load22}]. \end{split}$$

The controller bank of the UAC includes the following controllers, $c_1=(2-z^{-1})/(1-z^{-1})$, $c_2=(0.5+0.4z^{-1})/(1-z^{-1})$. Controller c_1 and c_2 are the stabilizing controllers

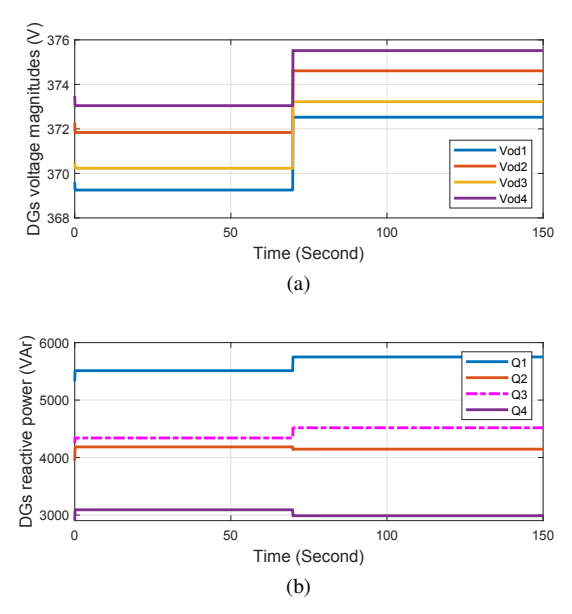


Fig. 11. UAC Results for Case Study A4 with failure in all DG that has acces to v_{ref} : (a) DGs' voltage magnitudes; (b) DGs' reactive powers.

designed for loads RX_1 and RX_2 , respectively. The initial active controller is c_1 .

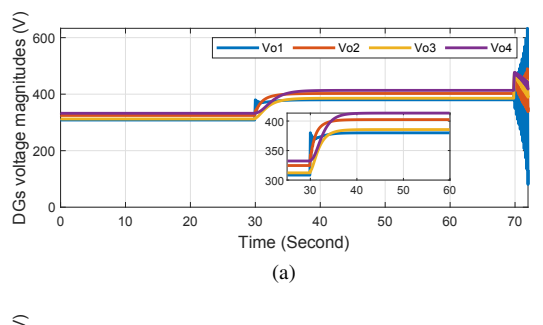
The result of using the conventional distributed secondary voltage control are shown in Fig. 12a. As seen, after load change at t=69.9 s, the conventional method fails to keep the microgrid's voltages stable. Then, it is assumed that UAC is located on DG1 with λ_0 set to 0.1. The simulation results for this case are provided in Figs. 12b, 12c, and 12d. After islanding between t=29.9 s and t=69.9 s, the controller c_1 is the stabilizer controller. After t=69.9 s, when the microgrid load decreases, the controller c_1 is no longer the stabilizing controller. At t=69.9 s, the UAC notices the instability in the microgrid, and, at t=70 s, the active controller is changed to the controller c_2 . The controller c_2 is the stabilizer controller for the load RX_2 .

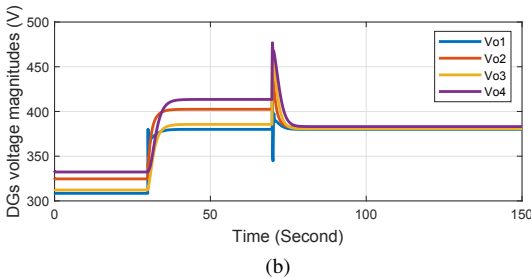
The results of the proposed method when parameter λ_0 is equal to 0.7 are provided in Fig. 13. As seen, with this λ_0 , UAC is slower than the case of λ_0 equal to 0.1. The UAC notices the instability 0.4 s after the load change occurs and replaces the active controller with a stabilizer controller in t=70.3 s.

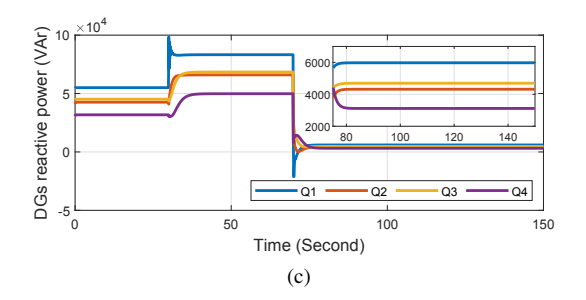
6) Case Study A6 - UAC with Load Change and communication failure and delay: Assuming a load change scenario similar to Case Study A5, the performance of the proposed method against the communication failure and delay is verified in Fig. 14. The load change occurs at $t=69.9~\rm s$. The stabilizing controllers are similar to the ones in Case Study A4. The communication failure and delay scenario is similar to Case Study A3 in Section V.A.3. Fig. 14 shows that UAC can effectively work in the presence of load change and communication failure and delay.

B. Case Study B

The microgrid test system for Case Study B is shown in Fig. 15. The communication graph for the secondary distributed







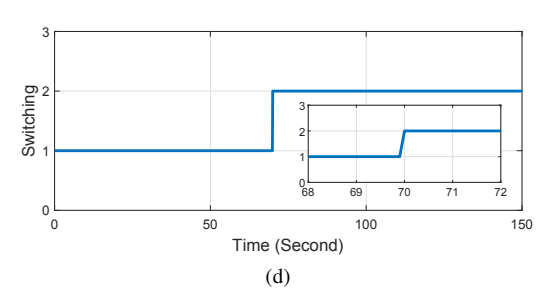


Fig. 12. Results for Case Study A5: (a) DGs' voltage magnitudes using conventional control; (b) DGs' voltage magnitudes using UAC on DG1 with $\lambda_0=0.1$; (c) DGs' reactive powers using UAC on DG1 with $\lambda_0=0.1$; (d) controller switching instance using UAC on DG1 with $\lambda_0=0.1$.

control and the parameters of the microgrid are provided in Fig. 16 and Table. II, respectively.

1) Case Study B1 - UAC with Voltage Droop Coefficient Change: The microgrid goes to islanding mode at t=17.94 s. UAC's controller bank includes two controllers, these two controllers are $c_1=(3-1.5z^{-1})/(1-z^{-1})$, $c_2=(1.65-0.15z^{-1})/(1-z^{-1})$. It is assumed that c_1 is designed for the voltage droop coefficients $[n_{Q11},n_{Q21},...,n_{Q201}]$ and c_2 is designed for the voltage droop coefficients $[n_{Q12},n_{Q22},...,n_{Q202}]$, which are provided in Table II. The parameter λ_0 in LICLA algorithm is set to 0.1.

Between t=17.94 s and t=41.94 s, it is assumed that the voltage droop coefficients of DGs are $[n_{Q11}, n_{Q21}, ..., n_{Q201}]$. At t=41.94 s, the voltage droop coefficients of DGs are

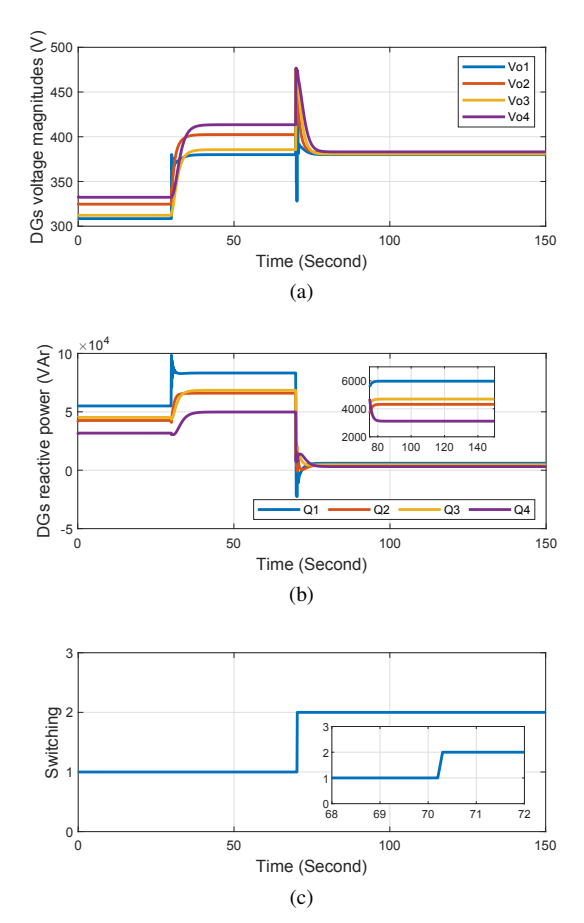


Fig. 13. UAC Results for Case Study A5 with $\lambda_0 = 0.7$: (a) DGs' voltage magnitudes; (b) DGs' reactive powers; (c) controller switching instance.

changed to $[n_{Q12}, n_{Q22}, ..., n_{Q202}]$. The initial active controller is c_1 . First, conventional secondary voltage control is considered. controller c_1 is used for the whole simulation. Between t=17.94 s and t=41.94 s, the controller c_1 results in a stable voltage regulation. But, after t=41.94 s, when the droop coefficients are changed to $[n_{Q12}, n_{Q22}, ..., n_{Q202}]$, the controller c_1 no longer accommodates a stable voltage regulation (see Fig. 17a). In the second scenario, the UAC is utilized which notices the instability at t=41.94 s and switches to controller c_2 at t=42 s fast enough before the microgrid stability margins are violated. The voltages, DGs' reactive powers, and controller switching instance are illustrated in Figs. 17b, 17c, and 17d, respectively. As seen, all the voltage magnitudes are stable and track the nominal value (380 V). Also, the reactive powers are in a stable range.

2) Case Study B2 - UAC with Load change: Consider the 20 DG microgrid with constant droop coefficients $[n_{Q11},n_{Q21},...,n_{Q201}]$ but with variable loads. It is assumed that the microgrid goes to islanding mode at t=17.94 s. Between t=0 s and t=119.94 s, it is assumed that the loads of the microgrid are RX_1 . At t=119.94 s, the loads are changed to RX_2 , where

$$RX_1 = [R_{load11}, ..., R_{load201}, X_{load11}, ..., X_{load201}],$$

$$RX_2 = [R_{load12}, ..., R_{load202}, X_{load12}, ..., X_{load202}].$$

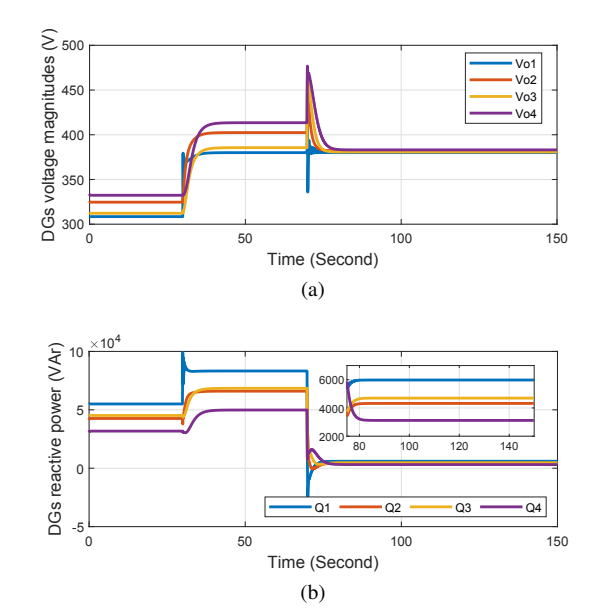


Fig. 14. UAC Results for Case Study A6 with communication link delay and failure: (a) DGs' voltage magnitudes; (b) DGs' reactive powers.

TABLE II THE PARAMETERS OF THE $20\ DG$ MICROGRID.

v_{nom}, f_{nom}	380 V, 50 Hz
$[m_{p1},,m_{p20}]$	9.4e - 5
Maximum active power of each load	207.1 kW
Maximum reactive power of each load	130 kVAr
$[R_{load11},,R_{load101}]$	0.5Ω
$[R_{load12},,R_{load102}]$	5Ω
$[X_{load11},, X_{load101}]$	0.314Ω
$[X_{load12},,X_{load102}]$	0.314Ω
$[n_{Q11},,n_{Q51}]$	[14, 23, 25, 26, 25]e - 4
$[n_{Q61},,n_{Q101}]$	[93, 28, 22, 23, 33]e - 4
$[n_{Q111},,n_{Q151}]$	[24, 3, 23, 24, 3]e - 4
$[n_{Q161},,n_{Q201}]$	[26, 31, 29, 29, 91]e - 4
$[n_{Q12},,n_{Q52}]$	[14, 23, 25, 26, 25]e - 5
$[n_{Q62},,n_{Q102}]$	[93, 28, 22, 23, 33]e - 5
$[n_{Q112},,n_{Q152}]$	[24, 30, 23, 24, 30]e - 5
$[n_{Q162},,n_{Q202}]$	[26, 31, 29, 29, 91]e - 5
$[r_{line1}, r_{line3},, r_{line19}]$	0.23Ω
$[r_{line2}, r_{line4},, r_{line20}]$	0.35Ω
$[x_{line1}, r_{line3},, x_{line19}]$	$3.1e - 4 \Omega$
$[x_{line2}, r_{line4},, x_{line20}]$	$1.8e - 3 \Omega$
$[K_{pv}, K_{pc}, K_{iv}, K_{ic}]$	[0.05, 10.5, 390, 16e3]
$[L_f, C_f, L_c]$	[1.35 mH, 50 μ F, 0.35 mH]

The controller bank of the UAC includes the following controllers, $c_1 = (1.35-1.2z^{-1})/(1-z^{-1}), c_2 = (0.4-0.3z^{-1})/(1-z^{-1})$. Controller c_1 and c_2 are the stabilizing controllers designed for loads RX_1 and RX_2 , respectively. The initial active controller is c_1 . The parameter λ_0 in LICLA algorithm is set to 0.01.

The result of the conventional method is presented in Fig. 18a. As seen, after the load change, the conventional method is unable to maintain voltage stability of microgrid. However, with UAC, the microgrid stability is maintained which is shown in Figs. 18b and 18c. As seen in Fig. 18d, after islanding, between $t=17.94\,\mathrm{s}$ and $t=119.94\,\mathrm{s}$, the controller c_1 is the stabilizing controller. After $t=119.94\,\mathrm{s}$ the microgrid loads are changed to RX_2 for which c_1 is no longer

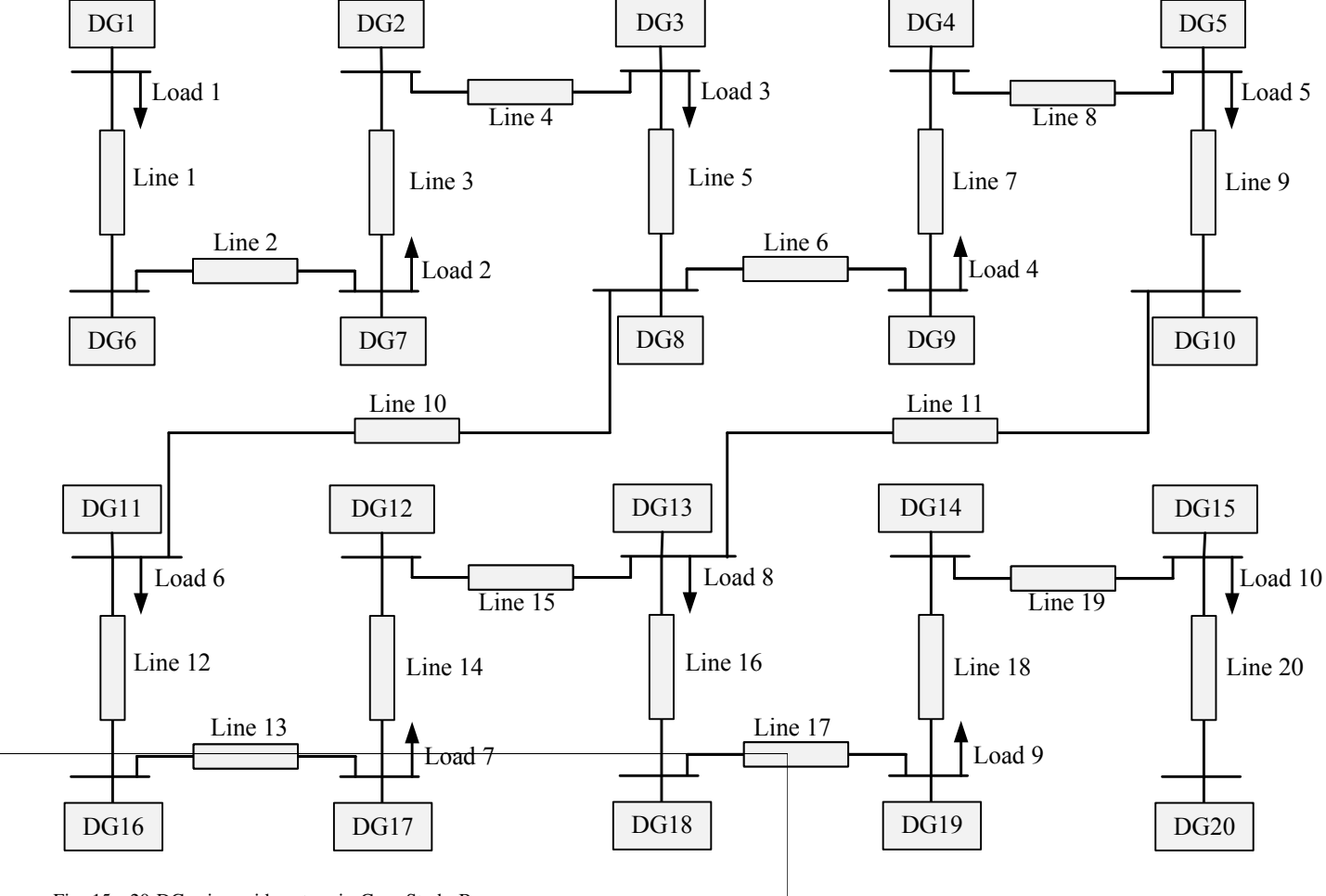


Fig. 15. 20 DG microgrid system in Case Study B.

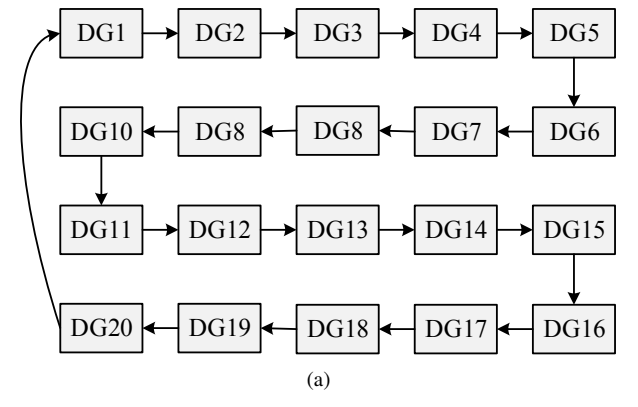


Fig. 16. Communication graph of 20 DG microgrid system in Case Study B.

stabilizer. At t=119.94 s, the UAC notices the instability in the microgrid and at t=120 s the active controller is changed to the controller c_2 . The controller c_2 is the stabilizer controller for loads RX_2 .

VI. CONCLUSION

This paper proposes a robust and adaptive voltage regulation technique for the secondary control of islanded inverter-based AC microgrids. To this end, a UAC-based approach is designed for the microgrid's distributed control system.

The UAC selects the best stabilizing controller from a set of pre-designed controllers with minimum knowledge required from the microgrid. A new cost-detectable cost function is proposed to account for the distributed and multi-agent nature of microgrids. Two microgrid test systems are simulated in MATLAB to verify the effectiveness of the proposed method under different conditions like load change, droop coefficient change, and communication delay and failure.

APPENDIX A PRELIMINARIES OF GRAPH THEORY

A graph is used to model the communication system of a microgrid. This graph can be defined by $\varsigma = (v, \varepsilon, A)$. v is a non-empty, finite set of Nv nodes. The nodes are connected by arcs or edges as $\varepsilon \subset v \times v$. Matrix A is an adjacency matrix with $A = [a_{ij}] \in R^{Nv \times Nv}$, where a_{ij} shows the weight of the edge (v_j, v_i) . If the node i receives information from the node j so the node j is called a neighbor of the node i and $(v_j, v_i) \in \varepsilon$. $N_i = \{j | (v_j, v_i) \in \varepsilon\}$ is a set that contains neighbors of the node i [6].

APPENDIX B PROOF OF THEOREM

To prove the stability of the secondary voltage control system with UAC, the cost function needs to be cost-detectable,

100

250

250

122

200

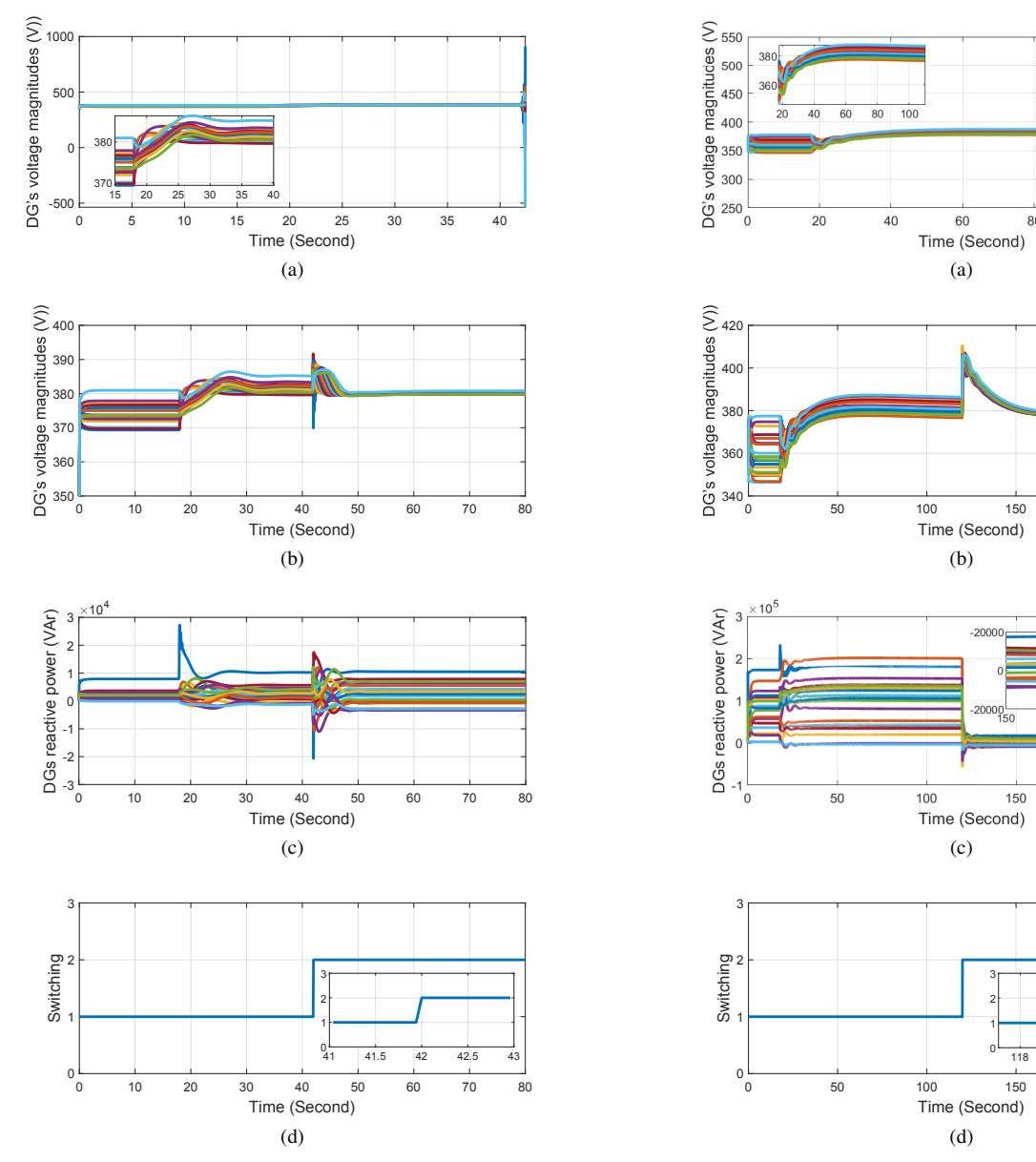


Fig. 17. Results for Case Study B1: (a) DGs' voltage magnitudes using conventional control; (b) DGs' voltage magnitudes using UAC on DG1; (c) DGs' reactive powers using UAC on DG1; (d) controller switching instance using UAC on DG1.

Fig. 18. Results for Case Study B2: (a) DGs' voltage magnitudes using conventional control; (b) DGs' voltage magnitudes using UAC on DG1; (c) DGs' reactive powers using UAC on DG1; (d) controller switching instance using UAC on DG1.

i.e., the cost function of the final controller in the loop, $\bar{V}_f(.)$, is bounded if and only if (p/c_f) is stable.

First, assume that the (p/c_f) is stable. According to the stability definition and the additivity feature of LTI systems one has

$$||u||_{[0,t]} + ||y||_{[0,t]} < m_0 ||r||_{[0,t]} + n_0 ||u||_{[0,t]} + ||y||_{[0,t]} < m_j ||v_{vcj}||_{[0,t]} + n_j \quad \forall j \in N_i$$
(14)

where u and y denote V_{ni} and v_{oi} , respectively. For $v_{vcj} = 0$,

$$\bar{V}_f(t) = \frac{\|\tilde{r}_f - y\|_{[0,t]} + \|u\|_{[0,t]}}{\alpha + \|\tilde{r}_f\|_{[0,t]} + \tilde{v}_{vc,f}}.$$
(15)

According to the triangle inequality one has

$$\bar{V}_f(t) < \frac{\|\tilde{r}_f\|_{[0,t]} + \|y\|_{[0,t]} + \|u\|_{[0,t]}}{\alpha + \|\tilde{r}_f\|_{[0,t]} + \tilde{v}_{vc,f}}.$$
 (16)

using (14) one has

$$\bar{V}_f(t) < \frac{\|\tilde{r}_f\|_{[0,t]} + m_0 \|r\|_{[0,t]} + n_0}{\alpha + \|\tilde{r}_f\|_{[0,t]} + \tilde{v}_{vc,f}}.$$
(17)

Since the final controller remains in the loop sufficiently enough, one can assume that $\tilde{r}_f \to r$ and $\tilde{v}_{vcj,f} \to v_{vcj} = 0, \forall j \in N_i$. Then, the rightmost term of above inequality can be rewritten as

$$\frac{\|r\|_{[0,t]} + m_0 \|r\|_{[0,t]} + n_0}{\alpha + \|r\|_{[0,t]}}$$
(18)

which is bounded and in turn makes $\bar{V}_f(t)$ bounded.

Similarly, assume that r=0, and v_{vcj} is only nonzero for one of the neighbors one at a time. Then, using triangle inequality and (14) one has

$$\bar{V}_f(t) < \frac{m_l \|v_{vcl}\|_{[0,t]} + n_l}{\alpha + \|\tilde{v}_{vcl,f}\|_{[0,t]}}$$
(19)

where l denotes the index of v_{vcl} that is nonzero. Since the final controller remains in the loop sufficiently enough, one can assume that $\tilde{v}_{vcj,f} \to v_{vcj} = 0$ for $j \neq l$, $\tilde{r}_f \to r = 0$ and $\tilde{v}_{vcl,f} \to v_{vcl}$. Then the rightmost term of above equation is bounded and $\bar{V}_f(t)$ is bounded. After repeating the above step in (19) for all of the neighbors of i^{th} DG, one can conclude that $\bar{V}_f(t)$ is bounded if (p/c_f) is stable.

Second, assume that the $\bar{V}_f(t)$ is bounded. Then,

$$\bar{V}_f(t) < K. \tag{20}$$

For $v_{vcj} = 0$,

$$\bar{V}_f(t) = \frac{\|r - y\|_{[0,t]} + \|u\|_{[0,t]}}{\alpha + \|r\|_{[0,t]}} < K \tag{21}$$

According to triangle inequality,

$$||y||_{[0,t]} + ||u||_{[0,t]} < K\alpha + K||r||_{[0,t]}$$
 (22)

which shows that (p/c_f) is stable according to the stability definition (14).

Similarly, assume that r=0, and v_{vcj} is only nonzero for one of the neighbors one at a time. Then, using triangle inequality

$$\bar{V}_f(t) = \frac{\|y\|_{[0,t]} + \|u\|_{[0,t]}}{\alpha + \|v_{vcl}\|_{[0,t]}}$$
(23)

$$||y||_{[0,t]} + ||u||_{[0,t]} < K\alpha + K||v_{vcl}||_{[0,t]}$$
 (24)

where l denotes the index of v_{vcl} that is nonzero. The above equation shows that (p/c_f) is stable according to the stability definition in (14). After repeating the above step one can conclude that (p/c_f) is stable if $\bar{V}_f(t)$ is bounded.

Therefore the proposed cost function is cost detectable. Since the pair of the controller bank and the cost function is cost-detectable, and the problem is feasible, so the proposed UAC system for microgrids distributed secondary voltage in Fig. 4a is stable.

REFERENCES

- [1] D. T. Ton and M. A. Smith, "The us department of energy's microgrid initiative," *The Electricity Journal*, vol. 25, no. 8, pp. 84–94, Oct. 2012.
- [2] C. Furlan and C. Mortarino, "Forecasting the impact of renewable energies in competition with non-renewable sources," *Renewable and Sustainable Energy Reviews*, vol. 81, pp. 1879–1886, Jan. 2018.
- [3] G. Dileep, "A survey on smart grid technologies and applications," Renewable Energy, vol. 146, pp. 2589–2625, Feb. 2020.
- [4] M. Farrokhabadi, C. A. Cañizares, J. W. Simpson-Porco, E. Nasr, L. Fan, P. A. Mendoza-Araya, R. Tonkoski, U. Tamrakar, N. Hatziargyriou, D. Lagos et al., "Microgrid stability definitions, analysis, and examples," *IEEE Trans. Power Systems*, vol. 35, no. 1, pp. 13–29, Jan. 2020.
- [5] A. Bidram and A. Davoudi, "Hierarchical structure of microgrids control system," *IEEE Trans. Smart Grid*, vol. 3, no. 4, pp. 1963–1976, Dec. 2012.
- [6] A. Bidram, A. Davoudi, and F. L. Lewis, "A multiobjective distributed control framework for islanded ac microgrids," *IEEE Trans. Industrial Informatics*, vol. 10, no. 3, pp. 1785–1798, Aug. 2014.

- [7] S. Abhinav, I. D. Schizas, F. Ferrese, and A. Davoudi, "Optimization-based ac microgrid synchronization," *IEEE Trans. Industrial Informatics*, vol. 13, no. 5, pp. 2339–2349, Oct. 2017.
- [8] D. E. Olivares, A. Mehrizi-Sani, A. H. Etemadi, C. A. Cañizares, R. Iravani, M. Kazerani, A. H. Hajimiragha, O. Gomis-Bellmunt, M. Saeedifard, R. Palma-Behnke et al., "Trends in microgrid control," *IEEE Trans. Smart Grid*, vol. 5, no. 4, pp. 1905–1919, July. 2014.
- [9] N. M. Dehkordi and S. Z. Moussavi, "Distributed resilient adaptive control of islanded microgrids under sensor/actuator faults," *IEEE Trans. Smart Grid*, vol. 11, no. 3, pp. 2699–2708, May. 2020.
- [10] J. Lai and X. Lu, "Nonlinear mean-square power sharing control for ac microgrids under distributed event detection," *IEEE Trans. Industrial Informatics*, vol. 17, no. 1, pp. 219–229, Jan. 2021.
- [11] A. Bidram, A. Davoudi, F. L. Lewis, and J. M. Guerrero, "Distributed cooperative secondary control of microgrids using feedback linearization," *IEEE Trans. Power Systems*, vol. 28, no. 3, pp. 3462–3470, Aug. 2013.
- [12] Y. Wang, T. L. Nguyen, M. H. Syed, Y. Xu, E. Guillo-Sansano, V.-H. Nguyen, G. M. Burt, Q.-T. Tran, and R. Caire, "A distributed control scheme of microgrids in energy internet paradigm and its multisite implementation," *IEEE Trans. Industrial Informatics*, vol. 17, no. 2, pp. 1141–1153, Feb. 2021.
- [13] M. Afrasiabi, M. Mohammadi, M. Rastegar, and A. Kargarian, "Multi-agent microgrid energy management based on deep learning forecaster," *Energy*, vol. 186, p. 115873, Nov. 2019.
- [14] A. Bidram, F. L. Lewis, and A. Davoudi, "Distributed control systems for small-scale power networks: Using multiagent cooperative control theory," *IEEE Control Systems Magazine*, vol. 34, no. 6, pp. 56–77, Dec. 2014.
- [15] R. de Azevedo, M. H. Cintuglu, T. Ma, and O. A. Mohammed, "Multiagent-based optimal microgrid control using fully distributed diffusion strategy," *IEEE Trans. Smart Grid*, vol. 8, no. 4, pp. 1997– 2008, July. 2017.
- [16] M. W. Khan, J. Wang, M. Ma, L. Xiong, P. Li, and F. Wu, "Optimal energy management and control aspects of distributed microgrid using multi-agent systems," *Sustainable Cities and Society*, vol. 44, pp. 855– 870, Jan. 2019.
- [17] Z. Ma, Z. Wang, Y. Guo, Y. Yuan, and H. Chen, "Secondary voltage control of microgrids using nonlinear multiple models adaptive control," arXiv preprint arXiv:1810.09577, Oct. 2018.
- [18] X. Lu, X. Yu, J. Lai, J. M. Guerrero, and H. Zhou, "Distributed secondary voltage and frequency control for islanded microgrids with uncertain communication links," *IEEE Trans. Industrial Informatics*, vol. 13, no. 2, pp. 448–460, April. 2017.
- [19] M. Mehdi, S. Z. Jamali, M. O. Khan, S. Baloch, and C.-H. Kim, "Robust control of a dc microgrid under parametric uncertainty and disturbances," *Electric Power Systems Research*, vol. 179, p. 106074, Feb. 2020.
- [20] Y. Xu, "Robust finite-time control for autonomous operation of an inverter-based microgrid," *IEEE Trans. Industrial Informatics*, vol. 13, no. 5, pp. 2717–2725, Oct. 2017.
- [21] G. Lou, W. Gu, Y. Xu, W. Jin, and X. Du, "Stability robustness for secondary voltage control in autonomous microgrids with consideration of communication delays," *IEEE Trans. Power Systems*, vol. 33, no. 4, pp. 4164–4178, July. 2018.
- [22] J.-O. Lee, Y.-S. Kim, and S.-I. Moon, "Novel supervisory control method for islanded droop-based ac/dc microgrids," *IEEE Trans. Power Systems*, vol. 34, no. 3, pp. 2140–2151, May. 2019.
- [23] M. G. Safonov and T.-C. Tsao, "The unfalsified control concept and learning," in *Proceedings of 33rd IEEE Conference on Decision and Control*, vol. 3, Dec. 1994, pp. 2819–2824.
- [24] R. Wang, A. Paul, M. Stefanovic, and M. Safonov, "Cost detectability and stability of adaptive control systems," *International Journal of Robust and Nonlinear Control: IFAC-Affiliated Journal*, vol. 17, no. 5-6, pp. 549–561, Mar. 2007.
- [25] C. Manuelli, S. G. Cheong, E. Mosca, and M. G. Safonov, "Stability of unfalsified adaptive control with non-scli controllers and related performance under different prior knowledge," in *European Control Conference (ECC)*, July. 2007, pp. 702–708.
- [26] S. Baldi, G. Battistelli, E. Mosca, and P. Tesi, "Multi-model unfalsified adaptive switching supervisory control," *Automatica*, vol. 46, no. 2, pp. 249–259, Feb. 2010.
- [27] S. Habibi, A. Khaki-Sedigh, and M. N. Manzar, "Performance enhancement of unfalsified adaptive control strategy using fuzzy logic," *International Journal of Systems Science*, vol. 50, no. 15, pp. 2752–2763, Oct. 2019.
- [28] H. Jin and M. Safonov, "Unfalsified adaptive control: Controller switching algorithms for nonmonotone cost functions," *International Journal*

- of Adaptive Control and Signal Processing, vol. 26, no. 8, pp. 692-704, Aug. 2012.
- [29] J. Rocabert, A. Luna, F. Blaabjerg, and P. Rodriguez, "Control of power converters in ac microgrids," *IEEE Trans. Power Electronics*, vol. 27, no. 11, pp. 4734–4749, Nov. 2012.
- [30] I. J. Balaguer, Q. Lei, S. Yang, U. Supatti, and F. Z. Peng, "Control for grid-connected and intentional islanding operations of distributed power generation," *IEEE Trans. Industrial Electronics*, vol. 58, no. 1, pp. 147–157, Jan. 2011.
- [31] M. Surprenant, I. Hiskens, and G. Venkataramanan, "Phase locked loop control of inverters in a microgrid," in *IEEE Energy Conversion Congress and Exposition*, Sept. 2011, pp. 667–672.
- [32] J. Wang, N. C. P. Chang, X. Feng, and A. Monti, "Design of a generalized control algorithm for parallel inverters for smooth microgrid transition operation," *IEEE Trans. Industrial Electronics*, vol. 62, no. 8, pp. 4900–4914, Aug. 2015.
- [33] J. Wang, A. Pratt, and M. Baggu, "Integrated synchronization control of grid-forming inverters for smooth microgrid transition," in *IEEE Power* & Energy Society General Meeting (PESGM), Aug. 2019, pp. 1–5.
- [34] J. Wang, B. Lundstrom, and A. Bernstein, "Design of a non-pll grid-forming inverter for smooth microgrid transition operation," in *IEEE Power & Energy Society General Meeting (PESGM)*, Aug. 2020, pp. 1–5.